Antarctic Ice Shelf Thickness Change from Multi-Mission Lidar Mapping

Tyler C. Sutterley[1], Thorsten Markus[1], Thomas A. Neumann[1], Michiel van den Broeke[2], J. Melchior van Wessem[2], and Stefan R. M. Ligtenberg[2]

[1]NASA Goddard Space Flight Center, Greenbelt, MD 20771
[2]Institute for Marine and Atmospheric Research, Utrecht University, Utrecht, The Netherlands

Correspondence: Tyler C. Sutterley (tyler.c.sutterley@nasa.gov)

Abstract.

We calculate rates of ice thickness change and bottom melt for ice shelves in West Antarctica and the Antarctic Peninsula from a combination of elevation measurements from Operation IceBridge corrected for oceanic and surface processes, surface velocity measurements from synthetic aperture radar, and high-resolution outputs from regional climate models. We calculate

5   ice thickness change rates in a Lagrangian reference frame to reduce the effects from advection of sharp vertical features, such as cracks and crevasses, which can saturate Eulerian-derived estimates. We use our method over different ice shelves in Antarctica, which vary in terms of the processes that drive their change, their size and their repeat coverage but are all susceptible to short-term changes in ice thickness. We find that ice thickness variations of the Larsen-C ice shelf are due to the flux divergence of the shelf with firn and surface processes controlling short-term variability over our observation period. The

10   Wilkins ice shelf is sensitive to short time-scale coastal and upper-ocean processes, and basal melt is the dominate contributor to the ice thickness change over the period. At The Pine Island ice shelf in the critical region near in the grounding zone, we find that ice shelf thinning rates exceed 40 m/yr. The thickness change is dominated by strong submarine thinning. Regions near the grounding zones of the Dotson and Crosson ice shelves are thinning at rates greater than 40 m/yr, also due to intense basal melt.

1 Introduction

15   Most of the drainage from the Antarctic ice sheet is through its peripheral ice shelves, floating extensions of the land ice that cover 75% of the Antarctic coastline and represent 10% of the total ice covered area (Cuffey and Paterson, 2010; Rignot et al., 2013). Floating ice shelves exert control on the grounded ice sheet's overall stability by buttressing the flow of the glaciers upstream (Dupont and Alley, 2005; Rignot et al., 2013). The thinning of Antarctic ice shelves reduces their ability to buttress

20   the glaciers that flow into them and makes the shelves more susceptible to fracture and overall collapse (Shepherd et al., 2003; Fricker and Padman, 2012). Ice shelves gain mass by the advection of ice from the land, the accumulation of snow at the surface, and the freezing of seawater at the ice shelf base (Thomas, 1979). They lose mass through runoff, wind scour and sublimation at the surface of the shelf, melting at the base of the shelf and through calving (Thomas, 1979).

Currently, several ice shelves across Antarctica are losing volume, which has led to the acceleration and intensified discharge of inland ice (Pritchard et al., 2012; Depoorter et al., 2013; Paolo et al., 2016). After the 2002 collapse of the Larsen B ice shelf, some tributary glaciers draining into the Weddell Sea from the Antarctic Peninsula accelerated 2 to 8 times their previous flow rates, and continued flowing at accelerated rates years after the collapse (Rignot et al., 2004, 2008; Berthier et al., 2012).

5   Glaciers of the Amundsen Sea Embayment (ASE) in West Antarctica have experienced significant increases in surface velocity, surface thinning, and grounding line retreat since the 1990's (Rignot et al., 2002, 2014; Pritchard et al., 2009). The internal change in ice dynamics of these glaciers likely stems from the advection of warm Circumpolar Deep Water, which enhanced ocean melt causing thinning of the buttressing peripheral ice shelves (Jacobs et al., 2011).

Here, we compile ice shelf thickness change rates calculated using a suite of airborne altimetry datasets, which have been

10 consistently processed and co-registered. The main objectives of this study are to (i) calculate ice shelf thickness change rates, (ii) investigate processes driving the changes in the shelf, (iii) investigate the sensitivity of spatial and temporal sampling to overall estimates and (iv) evaluate different methods of calculating elevation change rates over ice shelves. In the following sections, we discuss the co-registration method, the geophysical corrections applied, the results for a sample set of ice shelves and the overall implications of the results for ice shelf studies.

15 2   Materials and Methods

Our airborne lidar measurements are Level-2 Airborne Topographic Mapper (ATM Icessn) and Land, Vegetation and Ice Sensor (LVIS) datasets provided by the National Snow and Ice Data Center (NSIDC) (Thomas and Studinger, 2010; Studinger, 2014; Blair and Hofton, 2010). ATM is a conically scanning lidar which has flown in Antarctica since 2002 and was developed at the NASA Wallops Flight Facility (WFF) (Thomas and Studinger, 2010). LVIS is a large-swath scanning lidar which flew in

20 Antarctica in 2009, 2010, 2011 and 2015 and was developed at NASA Goddard Space Flight Center (GSFC) (Blair et al., 1999; Hofton et al., 2008). For the data release available for Antarctica (LDSv1), the Level-2 LVIS data provides 3 different elevation surfaces computed from the Level-1B waveforms: the highest and lowest returning surfaces from Gaussian decomposition, and the centroidal surface (Blair and Hofton, 2010). Here, we use the lowest returning surface when the waveform resembles a single-peak gaussian and the centroid surface when the waveform is multi-peak. The spatial coverage of each instrument in

25 Antarctica over Pre-IceBridge and NASA Operation IceBridge campaigns is shown in Figure 1. The elevation datasets from each instrument are converted to be in reference to the 2014 solution of the International Terrestrial Reference Frame (ITRF) (Altamimi et al., 2016). The ellipsoid heights for each instrument were converted into geoid heights using coefficients from the GGM05 gravity model provided by the Center for Space Research (Ries et al., 2016).

2.1   Integrated analysis of altimetry

30 We calculate rates of elevation change by comparing a set of measured elevation values with a set of interpolated elevation values from a different time period after allowing for the advection of the ice (Sutterley et al., 2018; Moholdt et al., 2014). Each point in a flight line is advected from its original location by integrating the Rignot et al. (2017) MEaSUREs velocity

data derived from synthetic aperture radar (SAR) using a fourth-order Runge-Kutta algorithm. For each data point in a flight line, a set of Delaunay triangles is constructed from a separate flight line using all data points within 300 meters from the final location of the advected point (Pritchard et al., 2009, 2012; Rignot et al., 2013). If the advected point lies within the confines of the Delaunay triangulation convex hull, the triangular facet housing the advected point is determined using a winding number

5   algorithm (Sutterley et al., 2018). The new elevation value is calculated using barycentric interpolation with the elevation measurements at the three triangle vertices (Figure 2).

Assuming that the ice shelf surfaces are not curved over the scale of the individual triangular facet, interpolating to the advected coordinates will compensate for minor slopes in the ice shelf surface so that the elevations of equivalent parcels of ice can be compared in time (Pritchard et al., 2009). At this scale (below 100–200m), the topographic relief of uncrevassed

10   ice is primarily due to slopes in the ice surface and a planar assumption should be largely valid (Markus et al., 2017). Rough terrain, snow drifts and low-lying clouds will contaminate the lidar elevation values for the interpolation. In order to limit the effect of contaminated points, the elevation measurements are filtered using the Robust Dispersion Estimator (RDE) algorithm described in Smith et al. (2017).

2.2 Geophysical Corrections

15   We correct the elevation measurements for geophysical processes following most of the procedures that will be used with ICESat-2 data (Markus et al., 2017; Neumann et al., 2018). The processes are described in the following sections and represented as a schematic in Figure 3.

2.2.1 Tidal and Non-Tidal Ocean Variation

Surface elevation changes due to variations in ocean and load tides are calculated using outputs from the Circum-Antarctic

20   Tidal Simulation (CATS2008) model (Padman et al., 2008), a high-resolution inverse model updated from Padman et al. (2002). Surface heights were predicted for the M_2, S_2, N_2, K_2, K_1, O_1, P_1, Q_1, M_f and M_m harmonic constituents and then inferred for 16 minor constituents following the *PERTH3* algorithm developed by Richard Ray at NASA Goddard Space Flight Center (GSFC) (Ray, 1999). We correct for changes in load and ocean pole tides due to changes in the Earth's rotation vector following Desai (2002) and IERS conventions (IERS). We correct for changes in sea surface height due to changes in atmo-

25   spheric pressure and wind stress using a dynamic atmosphere correction (DAC) provided by AVISO. The 6-hour DAC product combines outputs of the MOD2D-g ocean model, a 2-D ocean model forced by pressure and wind fields from ECMWF based on Lynch and Gray (1979), with an inverse barometer (IB) response (Legos; Carrère and Lyard, 2003). Non-tidal sea surface anomalies over ice-free ocean points are removed from the ice shelf data using multi-mission altimetry products computed by AVISO and provided by Copernicus (Le Traon et al., 1998; CMEMS).

2.2.2 Surface Mass Balance and Firn Compaction

After correcting for the effects of oceanic variation and advection, changes in surface height are due to a combination of accumulation, ablation and firn densification processes. To account for variations in surface elevation due to changes in surface processes, we use monthly mean surface mass balance (SMB) outputs calculated from climate simulations of the Regional Atmospheric Climate Model (RACMO2.3p2) computed by the Ice and Climate group at the Institute for Marine and Atmospheric Research of Utrecht University (IMAU) (Ligtenberg et al., 2013; van Wessem et al., 2014, 2018). We use 5.5km horizontal resolution outputs for the Antarctic Peninsula (XPEN055, van Wessem et al., 2016) and West Antarctica (ASE055, Lenaerts et al., 2018). The high-resolution outputs better represent the surface mass balance state than outputs from the 27km ice sheet wide model, particularly in the highly complex topography of mountains and glacial valleys in the Antarctic peninsula (van Wessem et al., 2016, Figure 4). SMB is the quantified difference between mass inputs from the precipitation of snow and rain, and mass losses by sublimation, runoff, and wind scour (Lenaerts et al., 2012; van den Broeke et al., 2009). Runoff is the portion of total snowmelt not retained or refrozen within the ice sheet. Wind scour is the erosion and sublimation of wind-blown snow from the ice sheet surface (Das et al., 2013). The absolute precision of the RACMO2.3p2 model outputs has been estimated using field data, such as ice cores and surface stake measurements (van de Berg et al., 2006). To correct for variations in the firn layer thickness, we use outputs from a semi-empirical firn densification model that simulates the steady-state firn density profile (Ligtenberg et al., 2011, 2012). The firn densification model is forced with surface mass balance outputs, surface temperatures fields and near-surface wind speed fields computed by RACMO2.3p2 (Ligtenberg et al., 2011).

2.3 Ice Shelf Bottom Melt

Changes in ice shelf mass in a Lagrangian reference frame are due to changes in surface mass balance (SMB) processes, basal melt and the divergence of the ice shelf flow field (Equation 1, Moholdt et al., 2014).

$$\frac{dM_{SMB}}{dt} + \frac{dM_b}{dt} - M\nabla \cdot V = \frac{\rho_w \rho_{ice}}{\rho_w - \rho_{ice}}\left(\frac{dh}{dt} - \frac{dh_{oc}}{dt} - \frac{dh_{fc}}{dt}\right) \tag{1}$$

We estimate ice shelf bottom melt rates along flight lines by using mass conservation and estimates of the mass flux divergence (Rignot and Jacobs, 2002; Moholdt et al., 2014; Rignot et al., 2013). Ice flow divergence fields are calculated from inSAR-derived ice velocities from Mouginot et al. (2017a) differentiated using a Savitzky-Golay filter with an 11 km half-width window (Savitzky and Golay, 1964). The Savitzky-Golay algorithm smoothes the velocity field, and reduces the impact of ionospheric noise and other sources of uncertainty on the differentials. We use ice thickness data from Bedmap2, which is primarily derived from Griggs and Bamber (2011) for ice shelves (Fretwell et al., 2013). The ice thickness estimates are calculated assuming hydrostatic equilibrium, which should be valid for areas 1–8 kilometers downstream of the grounding zone (Brunt et al., 2010, 2011).

3   Results

Figure 5 (a-b) shows the change in ice thickness of the Larsen-B and Larsen-C ice shelves for two periods, 2002–2008 and 2008–2016, from Pre-IceBridge and Operation IceBridge airborne data. Figure 5 (c-d) shows the estimated basal thickness change rate of the ice shelves over the same periods. The average thickness change rate between 2008 and 2016 from the flight line data over the Larsen-C ice shelf is –1.4±0.6 m/yr. From 2008–2016, the strongest thinning occurs near the grounding zone, particularly for the flight lines starting near Cabinet and Mill Inlets. For a flight line starting near the Whirlwind Inlet, the ice shelf is thinning near the grounding zone at 2 m/yr (Figure 6a). Scatter in the ice thickness change rate across the flight line is typically 30–50 cm/yr, or a 4–6 cm/yr error in the measured elevation change rate (Figure 6a). Most of the thickness change along this line is due to the flux divergence of the shelf. As the basal thickness change rate is calculated via mass conservation and the observed thinning rate largely matches the flux divergence, estimates of the basal melt rate of the Larsen-C ice shelf are highly dependent on the SMB flux estimate.

Figure 7 shows the change in ice thickness (a-b) and estimated basal thickness change rates (c-d) of the Wilkins ice shelf for two 3-year periods from 2008–2011 and 2011–2014. The Wilkins ice shelf is fed by glaciers on Alexander Island, which is located near the west coast of the Antarctic Peninsula and is the largest of the Antarctic islands. Wilkins ice shelf is sensitive to short time-scale coastal and upper-ocean processes (Padman et al., 2012) and ablates largely through basal melting (Rignot et al., 2013). Ice shelf extents are delineated from Landsat imagery provided courtesy of the U.S. Geological Survey (LPDAAC) and MODIS imagery provided by NSIDC (Scambos et al., 2001). The delineations were manually digitized as the ice shelf is heavily crevassed in regions near the ice edge and the bay is often filled with ice mélange (Figure 7). The extent of the ice shelf reduced by over 6000 km^2 between 1990 and 2017 (Scambos et al., 2009). The partial collapse occurred once the shelf started decoupling from Charcot Island (Vaughan et al., 1993) and likely occurred due to hydro-fracturing (Scambos et al., 2009). Meltwater ponds covered areas of 300–600 km^2 in Landsat imagery in 1986 and 1990 (Vaughan et al., 1993). The ponds existed largely in the now-collapsed portions of the shelf near Rothschild Island. Average thinning rates of the Wilkins ice shelf from the flight lines were 1.2±0.4 m/yr from 2008–2011 and 0.7±0.4 m/yr from 2011–2014. Average estimated basal thickness change rates from the flight lines were 2.8±0.3 m/yr in the earlier period and 2.0±0.3 m/yr in the latter period. Basal accretion could have occurred in some regions during the 2011–2014 period.

Figure 8 shows the change in ice thickness (a-b) and estimated basal thickness change rates (c-d) of the Pine Island ice shelf for two periods from 2009–2011 and 2011–2015. These periods were chosen to include repeat measurements from LVIS of the ice shelf near the grounding zone and to use the high-resolution outputs of RACMO2.3p2 ASE055. In the previously grounded region between the 1996 and 2011 grounding lines, the ice shelf thinning rates were 97±15 m/yr during 2009–2011 and 82±7 m/yr during 2011–2015. Ice thickness change rates outside of the previously grounded area are significantly weaker, averaging –21±7 m/yr for 2009–2011 and –15±3 m/yr for 2011–2015. The average ice thinning rates from the flight lines were insignificantly different at 36±9 m/yr over 2009–2011 and 34±5 m/yr over 2011–2015. Basal melt rates near the grounding zone have the highest impact on the glacial flow dynamics (Rignot and Jacobs, 2002). The difference in melt rates near the grounding zone between 2009–2011 and 2011–2015 could possibly explain some of the moderation in thinning of the

grounded ice and stability in ice discharge from Pine Island Glacier after 2010 (McMillan et al., 2014; Medley et al., 2014). As shown in Figure 8b, the ice thickness change is dominated by strong submarine thinning, which is further evidence of the dominant oceanic controls on the ice shelf mass balance in this region (Rignot, 2002).

Ice thickness change rates (a-b) and estimated basal thickness change rates (c-d) of the Dotson and Crosson ice shelves for
5 two periods from 2002–2010 and 2010–2015 are shown in Figure 9. The glaciers flowing into the Dotson and Crosson ice shelves have rapidly thinned, increased in speed and experienced significant retreats of grounding line positions over the past 20 years (Mouginot et al., 2014; Scheuchl et al., 2016). Flow speeds of the Crosson ice shelf have doubled in some regions over 1996 to 2014, while the flow speed of Dotson has remained largely steady (Lilien et al., 2018). Regions near the grounding lines of the input glaciers are thinning rapidly for both shelves driven by strong basal melt. Basal thinning rates averaged 46–71
10 m/yr near the grounding zone of Smith glacier over the two periods. Khazendar et al. (2016) documented rapid submarine ice melt and the loss of 300–490 m of floating ice between 2002 and 2009. Our work here provides independent evidence of this large-scale melt using a separate method and more years of data. We find that the ice mass wastage continued unabated between 2010 and 2015 with thinning rates over the flight lines averaging 22±1 m/yr.

4 Discussion

15 Using a Lagrangian reference frame produces estimates of ice shelf thickness change with much less noise compared with a Eulerian reference frame (Moholdt et al., 2014, Figure 10). The advection of ice thickness gradients, such as that from cracks and crevasses in the ice, can saturate the Eulerian-derived estimates (Moholdt et al., 2014). Our Eulerian approach uses the same Triangulated Irregular Networks (TINs) technique but keeps the point measurement locations static. The Eulerian scheme is similar to the methods of Pritchard et al. (2012) and Rignot et al. (2013) that used ICESat data and required spatial smoothing
20 of the elevation change rates to filter out the effects of advected surface roughness. Moholdt et al. (2014) showed a similar improvement when comparing Lagrangian and Eulerian-derived estimates in bottom melt for the Ross and Filchner-Ronne ice shelves. In their study, Moholdt et al. (2014) used ICESat data integrated using an overlapping footprints scheme.

Lagrangian tracking of airborne data requires 1) a sufficiently wide scanning swath, 2) accurate flow-line flight planning or 3) dense grid measurements. With the current Operation IceBridge data at most locations, cross-flow flight lines advected
25 outside of the swath width over multi-year repeat times. This limited our dataset to regions with flow-line measurements, such as the Larsen-C ice shelf (Figure 5), or frequent measurements, such as the Dotson and Crosson ice shelves (Figure 9). For most ice shelves, the airborne data are too sparse to extract large-scale spatial trends, particularly in the era before Operation IceBridge. Isolated crossovers can be calculated using Lagrangian tracking for some ice shelves using along-flow and cross-flow measurements from separate years. However, these individual crossovers would likely not be representative of
30 the large-scale behavior of the ice shelf. Satellite altimetry measurements from ICESat-2 (Markus et al., 2017) should help rectify the data limitation problem by providing dense point clouds which could be combined with photogrammetric digital elevation models (DEMs) to create ice shelf-wide thickness change maps. A more comprehensive update from the ICESat results of Pritchard et al. (2012) and Rignot et al. (2013) will be possible once ICESat-2 data become available.

Here, the airborne data are co-registered in a Lagrangian reference frame using a static velocity map provided by NSIDC through the MEaSUREs program (Rignot et al., 2017). However, there are cases that do not fit the assumption of temporally-invariant velocities. Prior to the calving event of the 40,000 km^2 A-68 iceberg from the Larsen-C ice shelf on July 11, 2017, the ice was rifting from the south and the regions downstream of the crack were rotating outward (Hogg and Gudmundsson, 2017,

5 Figure 5). In the Amundsen Sea Embayment, the ice velocity structure has changed year-to-year since the 1990's (Rignot et al., 2008; Mouginot et al., 2014). The floating ice shelves in the Amundsen Sea are also rifting concurrently with the acceleration of the instreaming glaciers (Macgregor et al., 2012). For both of these cases, it would be more appropriate to predict the advected parcel location using a velocity time series. However, the spatial coverage of annual velocity maps is lacking for some time periods, which will complicate the advection calculation. With the high-temporal resolution data from

10 the ESA Sentinel mission, the Landsat-based goLIVE project and the future NASA-ISRO SAR mission (NISAR), the advected parcel locations could be predicted with much greater accuracy for recent Operation IceBridge campaigns and future altimetry missions.

This work builds off of the work of Paolo et al. (2015) and Adusumilli et al. (2018) that used radar altimetry data to analyze the recent thinning and basal melt rates of ice shelves. Paolo et al. (2015) calculated changes in the ice thickness time series over

15 an 18-year time period using a suite of satellite radar altimetry data compiled in an Eulerian frame of reference. They found that the overall volume loss of ice shelves accelerated over the period 1994–2012, particularly for the ice shelves of West Antarctica. Adusumilli et al. (2018) expanded on this work to estimate the basal melt rates over 23 years and including radar altimetry data from CryoSat-2. Our study provides a validation dataset for floating ice shelves using high-resolution airborne laser altimetry data. Laser altimeters and radar altimeters can measure different surfaces over snow-covered ice surfaces (Rémy and Parouty,

20 2009). Variations in the dielectric properties of the snow due to variable temperatures and snow grain sizes can affect the radar penetration depth (Rémy and Parouty, 2009). Determining the sensitivity of radar estimates to surface penetration over different surface types could help reconcile differences between the various estimates.

Compiling estimates of elevation change from laser altimetry is non-trivial and different processing methods can produce differing results. Felikson et al. (2017) compared four different processing schemes (crossover differencing, along-track surface

25 fits, overlapping footprints and triangulated irregular networks) using ICESat data in an Eulerian sense over grounded ice in Greenland. They found discernible and irreconcilable differences between methods when deriving elevation change over the grounded ice sheet. We compare results from overlapping footprints and triangulated irregular networks, the two methods most applicable to airborne data, to test their coherence over ice shelf surfaces. As the surface slopes on ice shelves are small, we find that overlapping footprints and TINs approaches produce similar estimates of elevation change with scanning lidars in

30 Lagrangian frames of reference (Figure 10). The overlapping footprints approach produces a slightly noisier but statistically similar estimate compared with the TINs approach, and is a significantly simpler algorithm to implement.

5 Conclusions

We present a method for measuring ice shelf thickness change through the co-registration of Operation IceBridge laser altimetry data in a Lagrangian reference frame. We use our method to detect changes in ice shelves in West Antarctica and the Antarctic Peninsula where the airborne data are available. We find that our method is a significant improvement over Eulerian-derived estimates that require substantial smoothing or spatial averaging of the data. However, there are significant limitations when using airborne data for detecting ice shelf thickness change with Lagrangian tracking, particularly the lower spatial coverage and typical lack of repeat tracks over ice shelves. Data from the recently launched NASA ICESat-2 mission will help rectify these problems, particularly if combined with high-resolution photogrammetric digital elevation models.

Code and data availability. NASA Operation IceBridge data are freely available from the National Snow and Ice Data Center (NSIDC) at http://nsidc.org/data/ILATM2/ for the Level-2 ATM data and http://nsidc.org/data/ILVIS2/ for the Level-2 LVIS data. NASA MEaSUREs INSAR-derived velocity maps are provided by NSIDC at https://nsidc.org/data/nsidc-0484. Bedmap2 ice thicknesses are provided by the British Antarctic Survey at https://www.bas.ac.uk/project/bedmap-2/. CATS2008 tidal constituents are available from the Earth & Space Research institute at https://www.esr.org/research/polar-tide-models/. The following programs are provided by this project for processing the Operation IceBridge data: *nsidc-earthdata* retrieves NASA data from NSIDC, *read-ATM1b-QFIT-binary* reads Level-1b Airborne Topographic Mapper (ATM) QFIT binary data products, *read-ATM2-icessn* reads Level-2 ATM Icessn data products and *read-LVIS2-elevation* reads Level-2 Land Vegetation and Ice Sensor (LVIS) data products.

Author contributions. T.C.S. performed the analysis and wrote the manuscript. T.M. and T.A.N. supervised the project and provided comments and feedback. M.v.d.B, S.R.M.L. and J.M.v.W. supplied the RACMO2.3p2 data and provided comments.

Competing interests. The authors declare that the research was conducted in the absence of any commercial or financial relationships that could be construed as a potential conflict of interest.

Acknowledgements. Research was supported by an appointment to the NASA Postdoctoral Program at NASA Goddard Space Flight Center, administered by Universities Space Research Association under contract with NASA. The authors wish to thank the editor and anonymous reviewers for their comments, Eric Rignot and Isabella Velicogna for their comments, Jeremie Mouginot for his advice on the laser altimetry analysis and members of the GSFC Cryospheric Sciences Laboratory for their comments and advice. The authors wish to acknowledge the NASA Operation IceBridge flight, instrument and science teams for their work to collect and produce the science data.

References

Adusumilli, S., Fricker, H. A., Siegfried, M. R., Padman, L., Paolo, F. S., and Ligtenberg, S. R. M.: Variable Basal Melt Rates of Antarctic Peninsula Ice Shelves, 1994–2016, Geophysical Research Letters, 45, 4086–4095, https://doi.org/10.1002/2017GL076652, https://doi.org/10.1002/2017GL076652, 2018.

5   Altamimi, Z., Rebischung, P., Métivier, L., and Collilieux, X.: ITRF2014: A new release of the International Terrestrial Reference Frame modeling nonlinear station motions, Journal of Geophysical Research: Solid Earth, 121, 6109–6131, https://doi.org/10.1002/2016JB013098, http://dx.doi.org/10.1002/2016JB013098, 2016JB013098, 2016.

Bamber, J. L., Gomez-Dans, J. L., and Griggs, J. A.: A new 1 km digital elevation model of the Antarctic derived from combined satellite radar and laser data – Part 1: Data and methods, The Cryosphere, 3, 101–111, https://doi.org/10.5194/tc-3-101-2009, http://www.the-cryosphere.
10   net/3/101/2009/, 2009.

Berthier, E., Scambos, T. A., and Shuman, C. A.: Mass loss of Larsen B tributary glaciers (Antarctic Peninsula) unabated since 2002, Geophysical Research Letters, 39, https://doi.org/10.1029/2012GL051755, http://doi.wiley.com/10.1029/2012GL051755, l13501, 2012.

Blair, J. B. and Hofton, M.: IceBridge LVIS L2 Geolocated Surface Elevation Product, NASA DAAC at the National Snow and Ice Data Center, Boulder, Colorado USA, http://dx.doi.org/10.5067/OIKFGJNBM6OO, version 2, 2010.

15   Blair, J. B., Rabine, D. L., and Hofton, M. A.: The Laser Vegetation Imaging Sensor: a medium-altitude, digitisation-only, airborne laser altimeter for mapping vegetation and topography, ISPRS Journal of Photogrammetry and Remote Sensing, 54, 115–122, https://doi.org/10.1016/S0924-2716(99)00002-7, http://www.sciencedirect.com/science/article/pii/S0924271699000027, 1999.

Brunt, K. M., Fricker, H. A., Padman, L., Scambos, T. A., and O'Neel, S.: Mapping the grounding zone of the Ross Ice Shelf, Antarctica, using ICESat laser altimetry, Annals of Glaciology, 51, 71–79, https://doi.org/10.3189/172756410791392790, https://doi.org/10.3189/
20   172756410791392790, 2010.

Brunt, K. M., Fricker, H. A., and Padman, L.: Analysis of ice plains of the Filchner–Ronne Ice Shelf, Antarctica, using ICESat laser altimetry, Journal of Glaciology, 57, 965–975, https://doi.org/10.3189/002214311798043753, http://dx.doi.org/10.3189/002214311798043753, 2011.

Carrère, L. and Lyard, F.: Modeling the barotropic response of the global ocean to atmospheric wind and pressure forcing - comparisons
25   with observations, Geophysical Research Letters, 30, https://doi.org/10.1029/2002GL016473, http://dx.doi.org/10.1029/2002GL016473, 1275, 2003.

CMEMS: Ssalto/Duacs altimeter products were produced and distributed by the Copernicus Marine and Environment Monitoring Service (CMEMS), http://www.marine.copernicus.eu, 2017.

Cuffey, K. M. and Paterson, W. S. B.: The Physics of Glaciers, Butterworth-Heinemann, Burlington, MA, 4th edn., http://www.elsevierdirect.
30   com/ISBN/9780123694614/The-Physics-of-Glaciers, 2010.

Das, I., Bell, R. E., Scambos, T. A., Wolovick, M., Creyts, T. T., Studinger, M., Frearson, N., Nicolas, J. P., Lenaerts, J. T. M., and van den Broeke, M. R.: Influence of persistent wind scour on the surface mass balance of Antarctica, Nature Geoscience, 6, 367–371, https://doi.org/10.1038/ngeo1766, http://www.nature.com/doifinder/10.1038/ngeo1766, 2013.

Depoorter, M. A., Bamber, J. L., Griggs, J. A., Lenaerts, J. T. M., Ligtenberg, S. R. M., van den Broeke, M. R., and Moholdt, G.: Calving
35   fluxes and basal melt rates of Antarctic ice shelves, Nature, 502, 89–92, https://doi.org/10.1038/nature12567, http://dx.doi.org/10.1038/
nature12567, 2013.

Desai, S. D.: Observing the pole tide with satellite altimetry, Journal of Geophysical Research: Oceans, 107, 7–1–7–13, https://doi.org/10.1029/2001JC001224, http://dx.doi.org/10.1029/2001JC001224, 3186, 2002.

Dupont, T. and Alley, R. B.: Assessment of the importance of ice-shelf buttressing to ice-sheet flow, Geophysical Research Letters, 32, https://doi.org/10.1029/2004GL022024, http://dx.doi.org/10.1029/2004GL022024, l04503, 2005.

5   Dutrieux, P., De Rydt, J., Jenkins, A., Holland, P. R., Ha, H. K., Lee, S. H., Steig, E. J., Ding, Q., Abrahamsen, E., and Schröder, M.: Strong Sensitivity of Pine Island Ice-Shelf Melting to Climatic Variability, Science, 343, 174–178, https://doi.org/10.1126/science.1244341, http://science.sciencemag.org/content/343/6167/174, 2014.

Felikson, D., Urban, T. J., Gunter, B. C., Pie, N., Pritchard, H. D., Harpold, R., and Schutz, B. E.: Comparison of Elevation Change Detection Methods From ICESat Altimetry Over the Greenland Ice Sheet, IEEE Transactions on Geoscience and Remote Sensing, PP, 1–12,
10   https://doi.org/10.1109/TGRS.2017.2709303, 2017.

Fretwell, P., Pritchard, H. D., Vaughan, D. G., Bamber, J. L., Barrand, N. E., Bell, R. E., Bianchi, C., Bingham, R. G., Blankenship, D. D., Casassa, G., Catania, G. A., Callens, D., Conway, H., Cook, A. J., Corr, H. F. J., Damaske, D., Damm, V., Ferraccioli, F., Forsberg, R., Fujita, S., Gim, Y., Gogineni, S. P., Griggs, J. A., Hindmarsh, R. C. A., Holmlund, P., Holt, J. W., Jacobel, R. W., Jenkins, A., Jokat, W., Jordan, T. A., King, E. C., Kohler, J., Krabill, W. B., Riger-Kusk, M., Langley, K. A., Leitchenkov, G., Leuschen, C., Luyendyk,
15   B. P., Matsuoka, K., Mouginot, J., Nitsche, F. O., Nogi, Y., Nost, O. A., Popov, S. V., Rignot, E. J., Rippin, D. M., Rivera, A., Roberts, J. L., Ross, N., Siegert, M. J., Smith, A. M., Steinhage, D., Studinger, M., Sun, B., Tinto, B. K., Welch, B. C., Wilson, D., Young, D. A., Xiangbin, C., and Zirizzotti, A.: Bedmap2: improved ice bed, surface and thickness datasets for Antarctica, The Cryosphere, 7, 375–393, https://doi.org/10.5194/tc-7-375-2013, http://www.the-cryosphere.net/7/375/2013/, 2013.

Fricker, H. A. and Padman, L.: Thirty years of elevation change on Antarctic Peninsula ice shelves from multimission satellite radar altimetry,
20   Journal of Geophysical Research: Oceans, 117, https://doi.org/10.1029/2011JC007126, http://dx.doi.org/10.1029/2011JC007126, c02026, 2012.

Griggs, J. A. and Bamber, J. L.: Antarctic ice-shelf thickness from satellite radar altimetry, Journal of Glaciology, 57, 485–498, https://doi.org/10.3189/002214311796905659, http://dx.doi.org/10.3189/002214311796905659, 2011.

Haran, T., Bohlander, J., Scambos, T., and Fahnestock, M.: MODIS Mosaic of Antarctica 2008-2009 (MOA2009) Image Map, NSIDC:
25   National Snow and Ice Data Center, Boulder, Colorado USA, https://doi.org/10.7265/N5KP8037, http://dx.doi.org/10.7265/N5KP8037, version 1, 2014.

Hofton, M. A., Blair, J. B., Luthcke, S. B., and Rabine, D. L.: Assessing the performance of 20–25 m footprint waveform lidar data collected in ICESat data corridors in Greenland, Geophysical Research Letters, 35, https://doi.org/10.1029/2008GL035774, http://dx.doi.org/10.1029/2008GL035774, l24501, 2008.

30   Hogg, A. E. and Gudmundsson, G. H.: Impacts of the Larsen-C Ice Shelf calving event, Nature Climate Change, 7, 540, https://doi.org/10.1038/nclimate3359, http://dx.doi.org/10.1038/nclimate3359, 2017.

IERS: IERS Conventions (2010), Tech. Rep. 36, International Earth Rotation and Reference Systems Service (IERS), Frankfurt am Main: Verlag des Bundesamts für Kartographie und Geodäsie, https://www.iers.org/IERS/EN/Publications/TechnicalNotes/tn36.html, 2010.

Jacobs, S. S., Jenkins, A., Giulivi, C. F., and Dutrieux, P.: Stronger ocean circulation and increased melting under Pine Island Glacier ice
35   shelf, Nature Geoscience, 4, 519–523, https://doi.org/10.1038/ngeo1188, http://dx.doi.org/10.1038/ngeo1188, 2011.

Khazendar, A., Rignot, E. J., Schroeder, D. M., Seroussi, H., Schodlok, M. P., Scheuchl, B., Mouginot, J., Sutterley, T. C., and Velicogna, I.: Rapid submarine ice melting in the grounding zones of ice shelves in West Antarctica, Nature Communications, 7, 13 243, https://doi.org/10.1038/ncomms13243, http://dx.doi.org/10.1038/ncomms13243, 2016.

Le Traon, P. Y., Nadal, F., and Ducet, N.: An Improved Mapping Method of Multisatellite Altimeter Data, Journal of Atmospheric and Oceanic Technology, 15, 522–534, https://doi.org/10.1175/1520-0426(1998)015<0522:AIMMOM>2.0.CO;2, http://dx.doi.org/10.1175/1520-0426(1998)015<0522:aimmom>2.0.co;2, 1998.

Legos: Dynamic atmospheric Corrections are produced by CLS Space Oceanography Division using the Mog2D model from Legos distributed by Aviso, with support from CNES, https://www.aviso.altimetry.fr/en/data/products/auxiliary-products/atmospheric-corrections.html, 2017.

Lenaerts, J. T. M., van den Broeke, M. R., van de Berg, W. J., van Meijgaard, E., and Kuipers Munneke, P.: A new, high-resolution surface mass balance map of Antarctica (1979–2010) based on regional atmospheric climate modeling, Geophysical Research Letters, 39, https://doi.org/10.1029/2011GL050713, http://dx.doi.org/10.1029/2011GL050713, l04501, 2012.

Lenaerts, J. T. M., Ligtenberg, S. R. M., Medley, B., Van de Berg, W. J., Konrad, H., Nicolas, J. P., Van Wessem, J. M., Trusel, L. D., Mulvaney, R., Tuckwell, R. J., Hogg, A. E., and Thomas, E. R.: Climate and surface mass balance of coastal West Antarctica resolved by regional climate modelling, Annals of Glaciology, 59, 29–41, https://doi.org/10.1017/aog.2017.42, https://www.cambridge.org/core/article/climate-and-surface-mass-balance-of-coastal-west-antarctica-resolved-by-regional-climate-modelling/E3DD6D0DA914C6031F96A548AF53603A, 2018.

Ligtenberg, S. R. M., Helsen, M. M., and van den Broeke, M. R.: An improved semi-empirical model for the densification of Antarctic firn, The Cryosphere, 5, 809–819, https://doi.org/10.5194/tc-5-809-2011, http://www.the-cryosphere.net/5/809/2011/, 2011.

Ligtenberg, S. R. M., Horwath, M., van den Broeke, M. R., and Legrésy, B.: Quantifying the seasonal "breathing" of the Antarctic ice sheet, Geophysical Research Letters, 39, https://doi.org/10.1029/2012GL053628, http://dx.doi.org/10.1029/2012GL053628, l23501, 2012.

Ligtenberg, S. R. M., Berg, W. J., van den Broeke, M. R., Rae, J. G. L., and van Meijgaard, E.: Future surface mass balance of the Antarctic ice sheet and its influence on sea level change, simulated by a regional atmospheric climate model, Climate Dynamics, 41, 867–884, https://doi.org/10.1007/s00382-013-1749-1, http://dx.doi.org/10.1007/s00382-013-1749-1, 2013.

Lilien, D. A., Joughin, I., Smith, B., and Shean, D. E.: Changes in flow of Crosson and Dotson ice shelves, West Antarctica, in, The Cryosphere, 12, 1415–1431, https://doi.org/10.5194/tc-12-1415-2018, https://www.the-cryosphere.net/12/1415/2018/, 2018.

LPDAAC: NASA Landsat Program, NASA EOSDIS Land Processes Distributed Active Archive Center (LP DAAC), USGS/Earth Resources Observation and Science (EROS) Center, Sioux Falls, South Dakota, https://lpdaac.usgs.gov/, 2017.

Lynch, D. R. and Gray, W. G.: A wave equation model for finite element tidal computations, Computers & Fluids, 7, 207–228, https://doi.org/10.1016/0045-7930(79)90037-9, http://www.sciencedirect.com/science/article/pii/0045793079900379, 1979.

Macgregor, J. A., Catania, G. A., Markowski, M. S., and Andrews, A. G.: Widespread rifting and retreat of ice-shelf margins in the eastern Amundsen Sea Embayment between 1972 and 2011, Journal of Glaciology, 58, 458–466, https://doi.org/10.3189/2012JoG11J262, http://dx.doi.org/10.3189/2012jog11j262, 2012.

Markus, T., Neumann, T., Martino, A., Abdalati, W., Brunt, K., Csatho, B., Farrell, S., Fricker, H., Gardner, A., Harding, D., Jasinski, M., Kwok, R., Magruder, L., Lubin, D., Luthcke, S., Morison, J., Nelson, R., Neuenschwander, A., Palm, S., Popescu, S., Shum, C., Schutz, B. E., Smith, B., Yang, Y., and Zwally, J.: The Ice, Cloud, and land Elevation Satellite-2 (ICESat-2): Science requirements, concept, and implementation, Remote Sensing of Environment, 190, 260–273, https://doi.org/10.1016/j.rse.2016.12.029, https://doi.org/10.1016/j.rse.2016.12.029, 2017.

McMillan, M., Shepherd, A., Sundal, A. V., Briggs, K. H., Muir, A., Ridout, A., Hogg, A., and Wingham, D.: Increased ice losses from Antarctica detected by CryoSat-2, Geophysical Research Letters, 41, 3899–3905, https://doi.org/10.1002/2014GL060111, http://dx.doi.org/10.1002/2014GL060111, 2014GL060111, 2014.

Medley, B., Joughin, I. R., Smith, B. E., Das, S. B., Steig, E. J., Conway, H., Gogineni, S. P., Lewis, C., Criscitiello, A. S., McConnell, J. R., van den Broeke, M. R., Lenaerts, J. T. M., Bromwich, D. H., Nicolas, J. P., and Leuschen, C.: Constraining the recent mass balance of Pine Island and Thwaites glaciers, West Antarctica, with airborne observations of snow accumulation, The Cryosphere, 8, 1375–1392, https://doi.org/10.5194/tc-8-1375-2014, http://www.the-cryosphere.net/8/1375/2014/, 2014.

5 Moholdt, G., Padman, L., and Fricker, H. A.: Basal mass budget of Ross and Filchner-Ronne ice shelves, Antarctica, derived from Lagrangian analysis of ICESat altimetry, Journal of Geophysical Research: Earth Surface, 119, 2361–2380, https://doi.org/10.1002/2014JF003171, http://dx.doi.org/10.1002/2014JF003171, 2014JF003171, 2014.

Mouginot, J., Rignot, E. J., and Scheuchl, B.: Sustained increase in ice discharge from the Amundsen Sea Embayment, West Antarctica, from 1973 to 2013, Geophysical Research Letters, 41, 1576–1584, https://doi.org/10.1002/2013GL059069, http://dx.doi.org/10.1002/2013GL059069, 2014.

10 Mouginot, J., Rignot, E., Scheuchl, B., and Millan, R.: Comprehensive Annual Ice Sheet Velocity Mapping Using Landsat-8, Sentinel-1, and RADARSAT-2 Data, Remote Sensing, 9, https://doi.org/10.3390/rs9040364, http://www.mdpi.com/2072-4292/9/4/364, 364, 2017a.

Mouginot, J., Scheuchl, B., and Rignot, E.: MEaSUREs Antarctic Boundaries for IPY 2007–2009 from Satellite Radar, NASA National Snow and Ice Data Center Distributed Active Archive Center, Boulder, Colorado USA, https://doi.org/10.5067/AXE4121732AD, http://dx.doi.org/10.5067/AXE4121732AD, version 2, 2017b.

15 Neumann, T., Brenner, A., Hancock, D., Robbins, J., and Saba, J.: Ice, Cloud, and land Elevation Satellite - 2 (ICESat-2) Project: Algorithm Theoretical Basis Document (ATBD) for Global Geolocated Photons (ATL03), Tech. rep., NASA Goddard Space Flight Center (GSFC), Greenbelt, MD, USA, https://icesatiimis.gsfc.nasa.gov, 2018.

Padman, L., Fricker, H. A., Coleman, R., Howard, S., and Erofeeva, L.: A new tide model for the Antarctic ice shelves and seas, Annals of Glaciology, 34, 247–254, https://doi.org/10.3189/172756402781817752, http://dx.doi.org/10.3189/172756402781817752, 2002.

20 Padman, L., Erofeeva, S. Y., and Fricker, H. A.: Improving Antarctic tide models by assimilation of ICESat laser altimetry over ice shelves, Geophysical Research Letters, 35, https://doi.org/10.1029/2008GL035592, http://dx.doi.org/10.1029/2008GL035592, l22504, 2008.

Padman, L., Costa, D. P., Dinniman, M. S., Fricker, H. A., Goebel, M. E., Huckstadt, L. A., Humbert, A., Joughin, I. R., Lenaerts, J. T. M., Ligtenberg, S. R. M., Scambos, T. A., and van den Broeke, M. R.: Oceanic controls on the mass balance of Wilkins Ice Shelf, Antarctica, Journal of Geophysical Research: Oceans, 117, https://doi.org/10.1029/2011JC007301, http://dx.doi.org/10.1029/2011JC007301, c01010, 2012.

Paolo, F. S., Fricker, H. A., and Padman, L.: Volume loss from Antarctic ice shelves is accelerating, Science, 348, 327–331, https://doi.org/10.1126/science.aaa0940, http://science.sciencemag.org/content/348/6232/327.abstract, 2015.

Paolo, F. S., Fricker, H. A., and Padman, L.: Constructing improved decadal records of Antarctic ice shelf height change from multiple satellite radar altimeters, Remote Sensing of Environment, 177, 192–205, https://doi.org/10.1016/j.rse.2016.01.026, http://linkinghub.elsevier.com/retrieve/pii/S0034425716300268, 2016.

Pritchard, H. D., Arthern, R. J., Vaughan, D. G., and Edwards, L. A.: Extensive dynamic thinning on the margins of the Greenland and Antarctic ice sheets, Nature, 461, 971–975, https://doi.org/10.1038/nature08471, http://www.nature.com/nature/journal/vaop/ncurrent/full/nature08471.html), 2009.

35 Pritchard, H. D., Ligtenberg, S. R. M., Fricker, H. A., Vaughan, D. G., van den Broeke, M. R., and Padman, L.: Antarctic ice-sheet loss driven by basal melting of ice shelves, Nature, 484, 502–505, https://doi.org/10.1038/nature10968, http://www.nature.com/doifinder/10.1038/nature10968, 2012.

Ray, R. D.: A global ocean tide model from Topex/Poseidon altimetry: GOT99.2, Tech. Rep. TM-1999-209478, NASA Goddard Space Flight Center, Greenbelt, MD, http://ntrs.nasa.gov/archive/nasa/casi.ntrs.nasa.gov/19990089548_1999150788.pdf, 1999.

Rémy, F. and Parouty, S.: Antarctic Ice Sheet and Radar Altimetry: A Review, Remote Sensing, 1, 1212–1239, https://doi.org/10.3390/rs1041212, http://www.mdpi.com/2072-4292/1/4/1212/, 2009.

5 Ries, J., Bettadpur, S., Eanes, R., Kang, Z., Ko, U., McCullough, C., Nagel, P., Pie, N., Poole, S., Richter, T., Save, H., and Tapley, B.: The Development and Evaluation of the Global Gravity Model GGM05, Tech. Rep. CSR-16-02, UTCSR, Austin, Texas, https://doi.org/10.5880/icgem.2016.002, ftp://ftp.csr.utexas.edu/pub/grace/GGM05/CSR-16-02.pdf, 2016.

Rignot, E.: Ice-shelf changes in Pine Island Bay, Antarctica, 1947–2000, Journal of Glaciology, 48, 247–256, https://doi.org/10.3189/172756502781831386, http://dx.doi.org/10.3189/172756502781831386, 2002.

10 Rignot, E. J. and Jacobs, S.: Rapid Bottom Melting Widespread near Antarctic Ice Sheet Grounding Lines, Science, 296, 2020–2023, https://doi.org/10.1126/science.1070942, http://www.sciencemag.org/cgi/doi/10.1126/science.1070942, 2002.

Rignot, E. J., Vaughan, D. G., Schmeltz, M., Dupont, T., and MacAyeal, D. R.: Acceleration of Pine Island and Thwaites Glaciers, West Antarctica, Annals of Glaciology, 34, 189–194, https://doi.org/10.3189/172756402781817950, http://dx.doi.org/10.3189/172756402781817950, 2002.

15 Rignot, E. J., Casassa, G., Gogineni, S. P., Krabill, W. B., Rivera, A., and Thomas, R. H.: Accelerated ice discharge from the Antarctic Peninsula following the collapse of Larsen B ice shelf, Geophysical Research Letters, 31, https://doi.org/10.1029/2004GL020697, http://dx.doi.org/10.1029/2004GL020697, l18401, 2004.

Rignot, E. J., Bamber, J. L., van den Broeke, M. R., Davis, C. H., Li, Y., van de Berg, W. J., and van Meijgaard, E.: Recent Antarctic ice mass loss from radar interferometry and regional climate modelling, Nature Geoscience, 1, 106–110, https://doi.org/10.1038/ngeo102,
20 http://www.nature.com/ngeo/journal/v1/n2/abs/ngeo102.html, 2008.

Rignot, E. J., Jacobs, S., Mouginot, J., and Scheuchl, B.: Ice-Shelf Melting Around Antarctica, Science, 341, 266–270, https://doi.org/10.1126/science.1235798, http://science.sciencemag.org/content/341/6143/266, 2013.

Rignot, E. J., Mouginot, J., Morlighem, M., Seroussi, H., and Scheuchl, B.: Widespread, rapid grounding line retreat of Pine Island, Thwaites, Smith, and Kohler glaciers, West Antarctica, from 1992 to 2011, Geophysical Research Letters, 41, 3502–3509,
25 https://doi.org/10.1002/2014GL060140, http://dx.doi.org/10.1002/2014GL060140, 2014.

Rignot, E. J., Mouginot, J., and Scheuchl, B.: MEaSUREs Antarctic Grounding Line from Differential Satellite Radar Interferometry, NASA National Snow and Ice Data Center Distributed Active Archive Center, Boulder, Colorado USA, https://doi.org/10.5067/IKBWW4RYHF1Q, http://dx.doi.org/10.5067/IKBWW4RYHF1Q, version 2, 2016.

Rignot, E. J., Mouginot, J., and Scheuchl, B.: MEaSUREs InSAR-Based Antarctica Ice Velocity Map, NASA National Snow and Ice Data
30 Center Distributed Active Archive Center, Boulder, Colorado USA, https://doi.org/10.5067/D7GK8F5J8M8R, http://dx.doi.org/10.5067/D7GK8F5J8M8R, version 2, 2017.

Savitzky, A. and Golay, M. J. E.: Smoothing and Differentiation of Data by Simplified Least Squares Procedures., Analytical Chemistry, 36, 1627–1639, https://doi.org/10.1021/ac60214a047, http://dx.doi.org/10.1021/ac60214a047, 1964.

Scambos, T., Raup, B. H., and Bohlander, J.: Images of Antarctic Ice Shelves, NASA National Snow and Ice Data Center Distributed Active
35 Archive Center, Boulder, Colorado USA, https://doi.org/10.7265/N5NC5Z4N, http://dx.doi.org/10.7265/N5NC5Z4N, version 1, 2001.

Scambos, T., Fricker, H. A., Liu, C.-C., Bohlander, J., Fastook, J., Sargent, A., Massom, R., and Wu, A.-M.: Ice shelf disintegration by plate bending and hydro-fracture: Satellite observations and model results of the 2008 Wilkins ice shelf break-ups, Earth and Planetary Science Letters, 280, 51–60, https://doi.org/10.1016/j.epsl.2008.12.027, http://dx.doi.org/10.1016/j.epsl.2008.12.027, 2009.

Scheuchl, B., Mouginot, J., Rignot, E. J., Morlighem, M., and Khazendar, A.: Grounding line retreat of Pope, Smith, and Kohler Glaciers, West Antarctica, measured with Sentinel-1a radar interferometry data, Geophysical Research Letters, 43, 8572–8579, https://doi.org/10.1002/2016GL069287, http://dx.doi.org/10.1002/2016GL069287, 2016GL069287, 2016.

Shepherd, A., Wingham, D. J., Payne, T., and Skvarca, P.: Larsen Ice Shelf Has Progressively Thinned, Science, 302, 856–859, https://doi.org/10.1126/science.1089768, http://science.sciencemag.org/content/302/5646/856, 2003.

Smith, B. E., Gourmelen, N., Huth, A., and Joughin, I.: Connected subglacial lake drainage beneath Thwaites Glacier, West Antarctica, The Cryosphere, 11, 451–467, https://doi.org/10.5194/tc-11-451-2017, http://www.the-cryosphere.net/11/451/2017/, 2017.

Studinger, M. S.: IceBridge ATM L2 Icessn Elevation, Slope, and Roughness, NASA National Snow and Ice Data Center Distributed Active Archive Center, Boulder, Colorado USA, https://doi.org/10.5067/CPRXXK3F39RV, http://dx.doi.org/10.5067/CPRXXK3F39RV, version 2, 2014.

Sutterley, T. C., Velicogna, I., Fettweis, X., Rignot, E., Noël, B., and Broeke, M.: Evaluation of Reconstructions of Snow/Ice Melt in Greenland by Regional Atmospheric Climate Models Using Laser Altimetry Data, Geophysical Research Letters, 45, 8324–8333, https://doi.org/10.1029/2018GL078645, https://doi.org/10.1029/2018GL078645, 2018.

Thomas, R. H.: Ice Shelves: A Review, Journal of Glaciology, 24, 273–286, https://doi.org/10.1017/S0022143000014799, https://www.cambridge.org/core/article/ice-shelves-a-review/A59D20319A6E15DB7A5C162BE4A0BF83, 1979.

Thomas, R. H. and Studinger, M. S.: Pre-IceBridge ATM L2 Icessn Elevation, Slope, and Roughness, NASA National Snow and Ice Data Center Distributed Active Archive Center, Boulder, Colorado USA, https://doi.org/10.5067/6C6WA3R918HJ, http://dx.doi.org/10.5067/6C6WA3R918HJ, version 1, 2010.

van de Berg, W. J., van den Broeke, M. R., Reijmer, C. H., and van Meijgaard, E.: Reassessment of the Antarctic surface mass balance using calibrated output of a regional atmospheric climate model, Journal of Geophysical Research: Atmospheres, 111, https://doi.org/10.1029/2005JD006495, http://dx.doi.org/10.1029/2005JD006495, d11104, 2006.

van den Broeke, M. R., Bamber, J. L., Ettema, J., Rignot, E. J., Schrama, E., van de Berg, W. J., van Meijgaard, E., Velicogna, I., and Wouters, B.: Partitioning Recent Greenland Mass Loss, Science, 326, 984–986, https://doi.org/10.1126/science.1178176, http://www.sciencemag.org/cgi/doi/10.1126/science.1178176, 2009.

van Wessem, J. M., Reijmer, C. H., Morlighem, M., Mouginot, J., Rignot, E. J., Medley, B., Joughin, I. R., Wouters, B., Depoorter, M. A., Bamber, J. L., Lenaerts, J. T. M., van de Berg, W. J., van den Broeke, M. R., and van Meijgaard, E.: Improved representation of East Antarctic surface mass balance in a regional atmospheric climate model, Journal of Glaciology, 60, 761–770, https://doi.org/10.3189/2014JoG14J051, http://dx.doi.org/10.3189/2014JoG14J051, 2014.

van Wessem, J. M., Ligtenberg, S. R. M., Reijmer, C. H., van de Berg, W. J., van den Broeke, M. R., Barrand, N. E., Thomas, E. R., Turner, J., Wuite, J., Scambos, T. A., and van Meijgaard, E.: The modelled surface mass balance of the Antarctic Peninsula at 5.5 km horizontal resolution, The Cryosphere, 10, 271–285, https://doi.org/10.5194/tc-10-271-2016, http://www.the-cryosphere.net/10/271/2016/, 2016.

van Wessem, J. M., van de Berg, W. J., Noël, B. P. Y., van Meijgaard, E., Amory, C., Birnbaum, G., Jakobs, C. L., Krüger, K., Lenaerts, J. T. M., Lhermitte, S., Ligtenberg, S. R. M., Medley, B., Reijmer, C. H., van Tricht, K., Trusel, L. D., van Ulft, L. H., Wouters, B., Wuite, J., and van den Broeke, M. R.: Modelling the climate and surface mass balance of polar ice sheets using RACMO2 – Part 2: Antarctica (1979–2016), The Cryosphere, 12, 1479–1498, https://doi.org/10.5194/tc-12-1479-2018, https://www.the-cryosphere.net/12/1479/2018/, 2018.

Vaughan, D. G., Mantripp, D. R., Sievers, J., and Doake, C. S.: A synthesis of remote sensing data on Wilkins Ice Shelf, Antarctica, Annals of Glaciology, 17, 211–218, https://doi.org/10.3189/S0260305500012866, http://dx.doi.org/10.3189/s0260305500012866, 1993.

Zwally, H. J. and Li, J.: Seasonal and interannual variations of firn densification and ice-sheet surface elevation at the Greenland sum-
    mit, Journal of Glaciology, 48, 199–207, https://doi.org/10.3189/172756502781831403, http://dx.doi.org/10.3189/172756502781831403,
    2002.
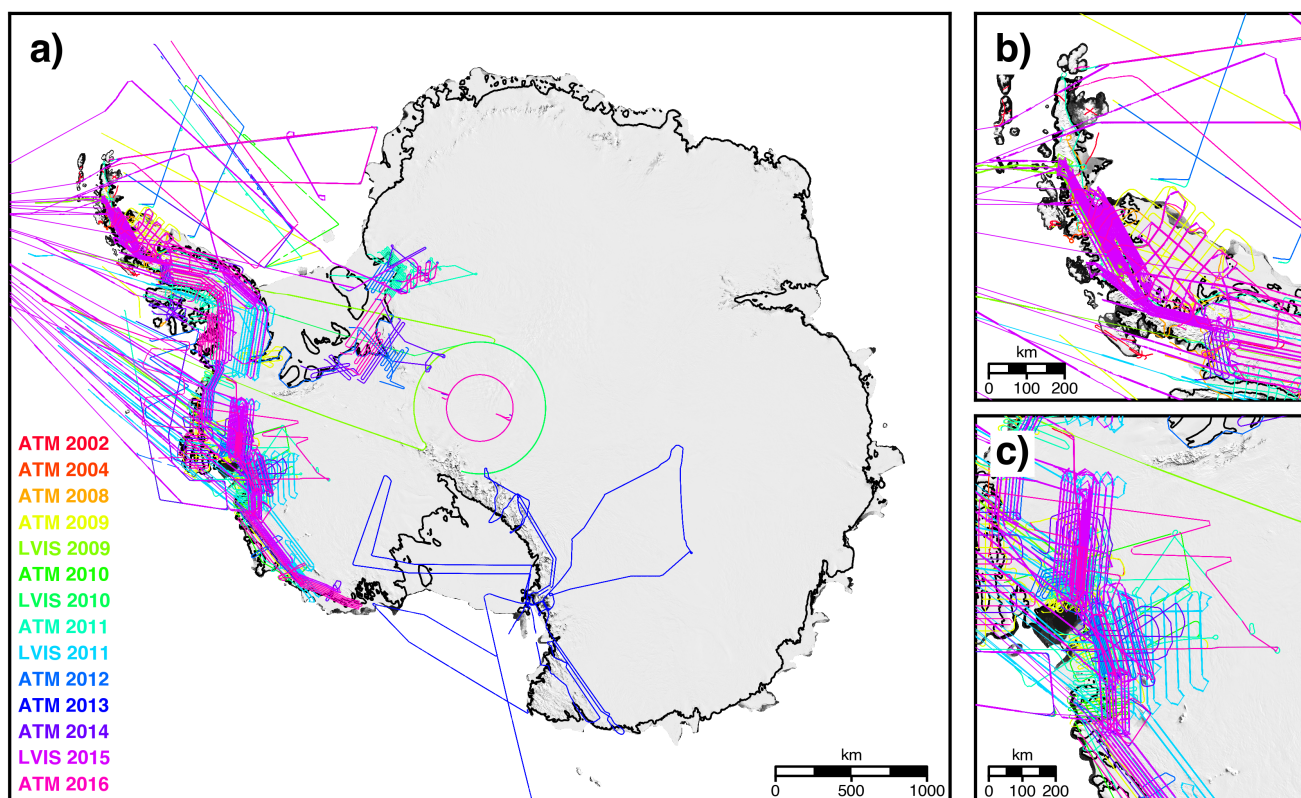
Figure 1. Pre-IceBridge and Operation IceBridge campaign flight lines over a) Antarctica b) the Antarctic Peninsula and c) the Amundsen
Sea Embayment from 2002 to 2016 colored by year of acquisition and laser ranging instrument. Antarctic grounded ice delineation provided
by Mouginot et al. (2017b). Flight lines overlaid on a 2008–2009 MODIS mosaic of Antarctica (Haran et al., 2014).
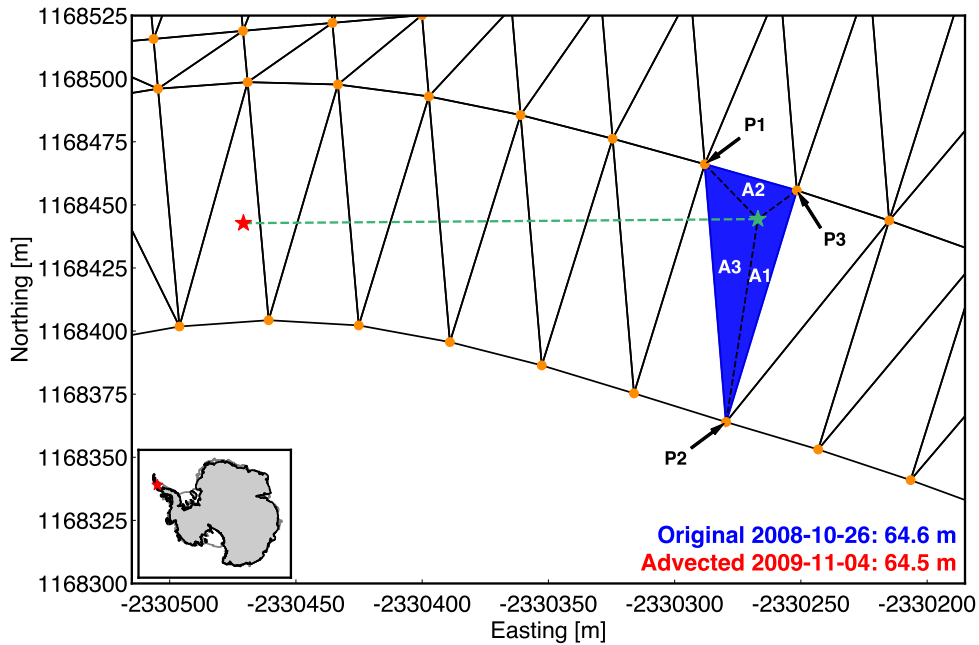
Figure 2. Triangulated mesh formulated around an advected 2008 ATM flight line point using points from a 2009 ATM flight line (orange dots). The red star denotes the location of the original point, the green star denotes the parcel location after advection, and the dashed green line is the path of advection. P1, P2 and P3 represent the three vertices of the triangle housing the advected ATM point. Elevation values at each vertex point are weighted in the interpolation by their respective areas, A1, A2 and A3. Inset map shows the location of the main figure.
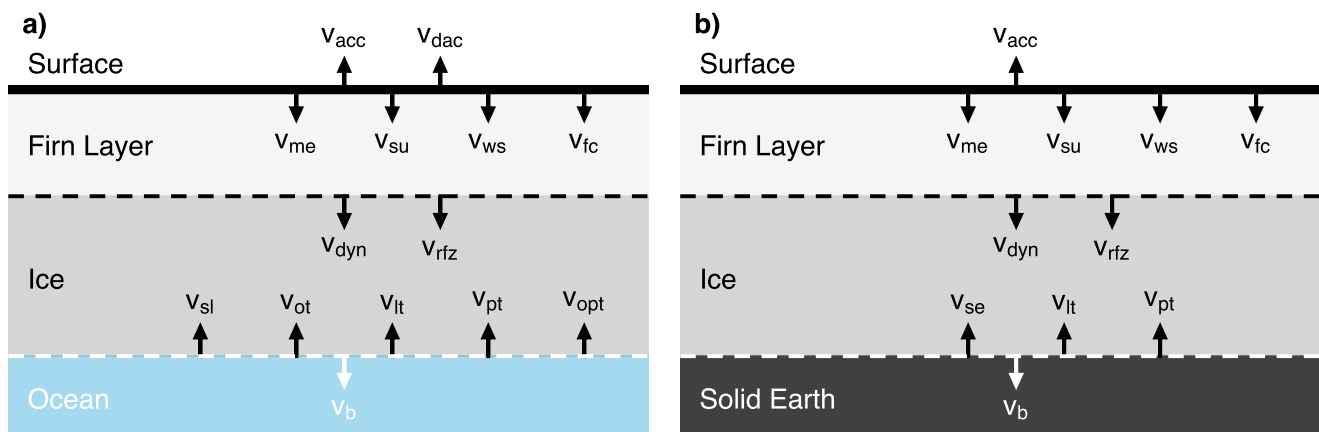
Figure 3. Representation of processes contributing to surface elevation changes for a) ice shelves and b) grounded ice. Modified from Ligtenberg et al. (2011) and Zwally and Li (2002). Processes represented in schematic: accumulation (v_{acc}), dynamic atmosphere (v_{dac}), snowmelt (v_{me}), sublimation (v_{su}), wind scour (v_{ws}), firn compaction (v_{fc}), ice dynamics (v_{dyn}), meltwater refreeze and retainment (v_{rfz}), solid Earth uplift (v_{se}), sea level (v_{sl}), ocean tides (v_{ot}), load tides (v_{lt}), load pole tides (v_{pt}), ocean pole tides (v_{opt}), and basal melt (v_b).
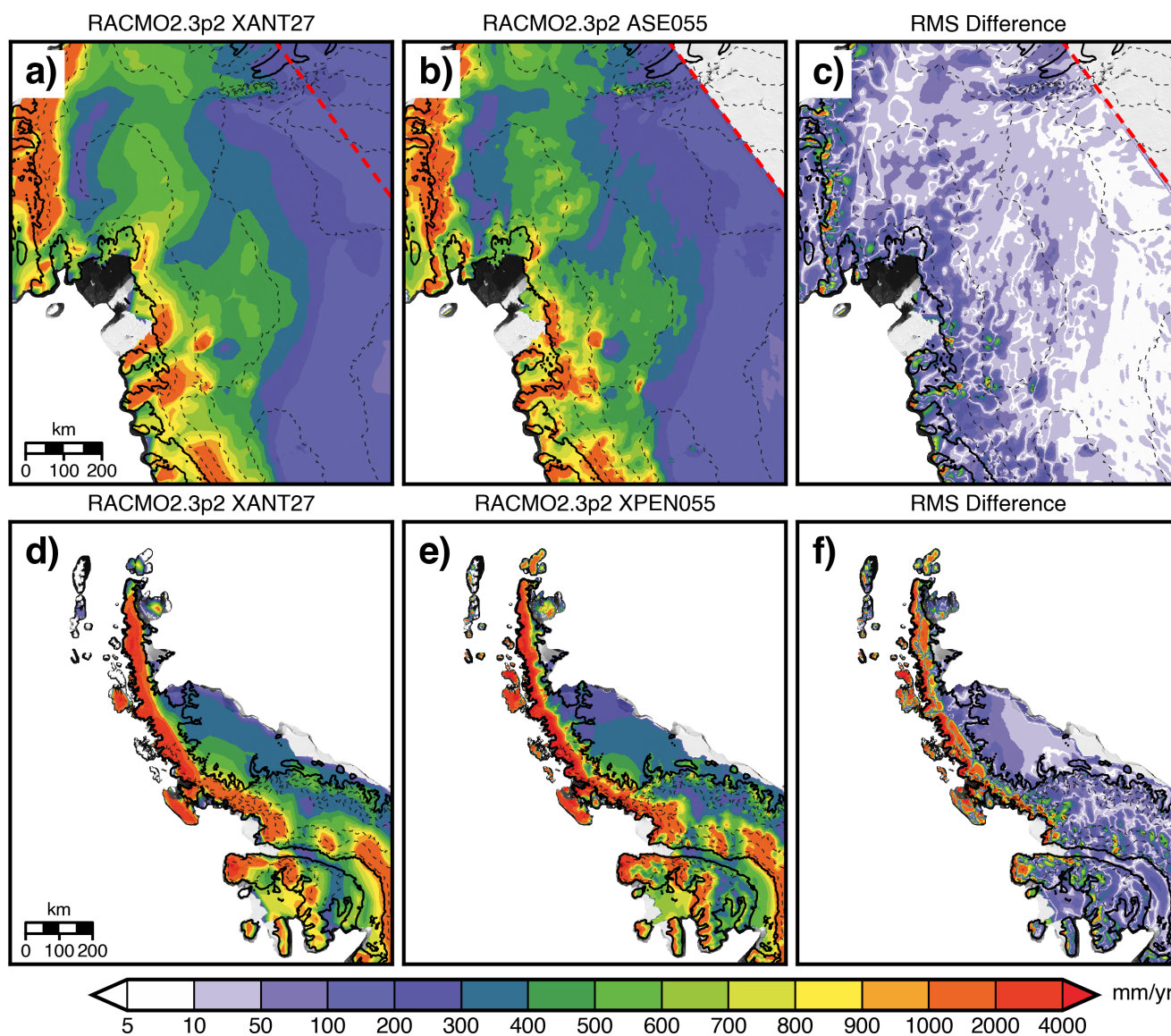
Figure 4. Mean 2002–2015 surface mass balance (SMB) from a,c) a 27km Antarctic-wide simulation b) a 5.5km Amundsen Sea Embayment simulation (ASE055), and d) a 5.5km Antarctic Peninsula simulation (XPEN055) of the Regional Atmospheric Climate Model (RACMO2.3p2) (van Wessem et al., 2014, 2016). RMS differences between c) Antarctic-wide and ASE055 solutions and f) Antarctic-wide and XPEN055 solutions. Thin black dashed lines denote 500m elevation contours from (Bamber et al., 2009). Thick red dashed line in a-c) denotes the boundary of the ASE055 model. Antarctic grounded ice boundaries are provided by Mouginot et al. (2017b). Plots are overlaid on a 2008–2009 MODIS mosaic of Antarctica (Haran et al., 2014).
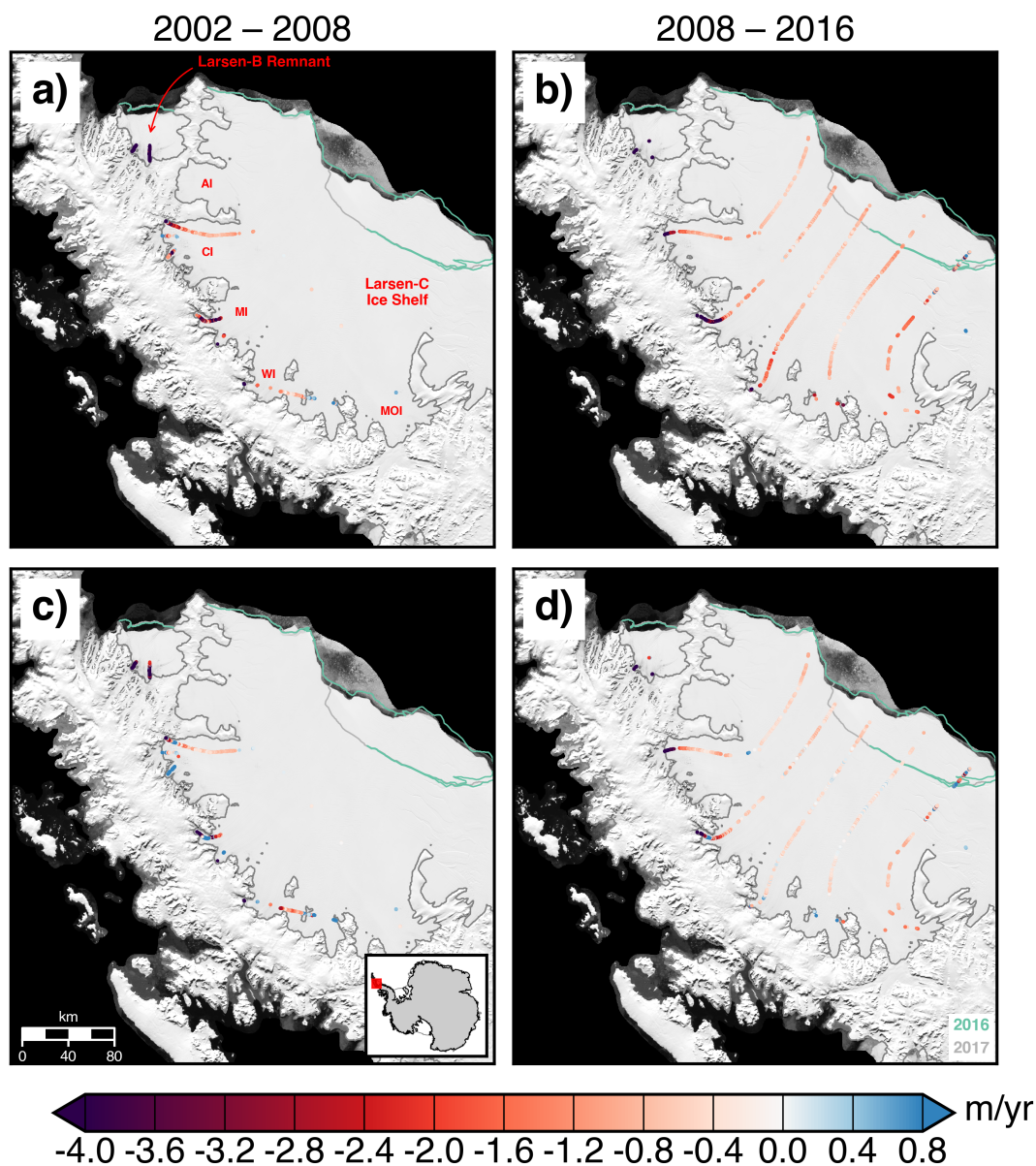
Figure 5. Ice thickness change (a-b) and estimated basal thickness change rates (c-d) of the Larsen-B remnant and Larsen-C ice shelf for two periods, 2002–2008 and 2008–2016. AI, CI, MI, WI and MOI denote the Adie, Cabinet, Mill, Whirlwind and Mobiloil inlets respectively. MEaSUREs InSAR-derived Antarctic grounded ice boundaries are denoted in gray (Mouginot et al., 2017b). 2016 and 2017 ice shelf extents delineated from MODIS imagery are denoted in green and light gray respectively (Scambos et al., 2001). Plots are overlaid on a 2008–2009 MODIS mosaic of Antarctica (Haran et al., 2014). Inset map denotes the location of the maps.
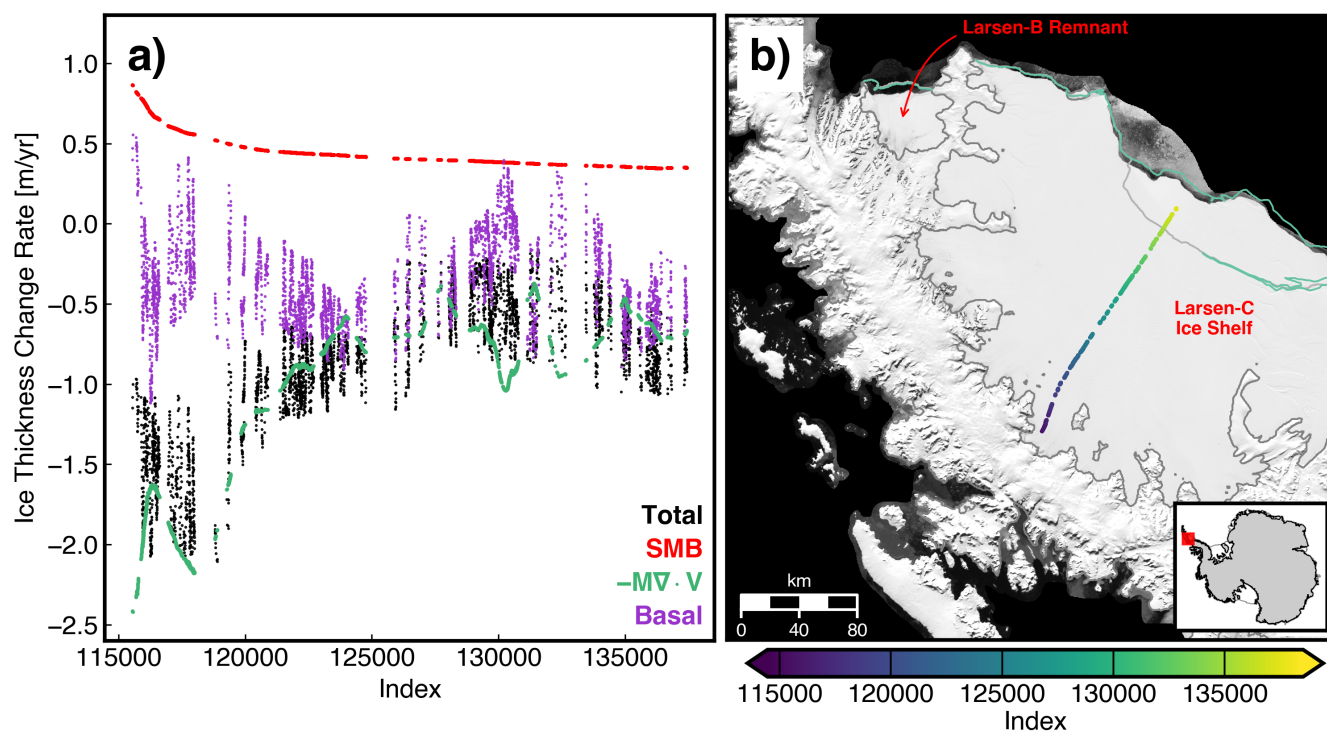
Figure 6. Measured and estimated ice thickness change rates from 2008 to 2016 for a flight line over the Larsen-C ice shelf (a) starting near the Whirlwind inlet with the total measured ice thickness change rate denoted in black, the surface mass balance (SMB) fluxes from RACMO2.3p2 (XPEN055) denoted in red (van Wessem et al., 2016), the flux divergence terms combining ice thicknesses from Bedmap2 (Fretwell et al., 2013) and ice velocities from MEaSUREs (Rignot et al., 2017) denoted in green and the residual basal thickness change rates denoted in purple. Index denotes the ATM Icessn record number for October 10, 2008. Locations of co-registered records from the flight line are shown in b). MEaSUREs InSAR-derived Antarctic grounded ice boundaries are denoted in gray (Mouginot et al., 2017b). 2016 and 2017 ice shelf extents delineated from MODIS imagery are denoted in green and light gray respectively (Scambos et al., 2001). Map is overlaid on a 2008–2009 MODIS mosaic of Antarctica (Haran et al., 2014). Inset map denotes the location of the map.
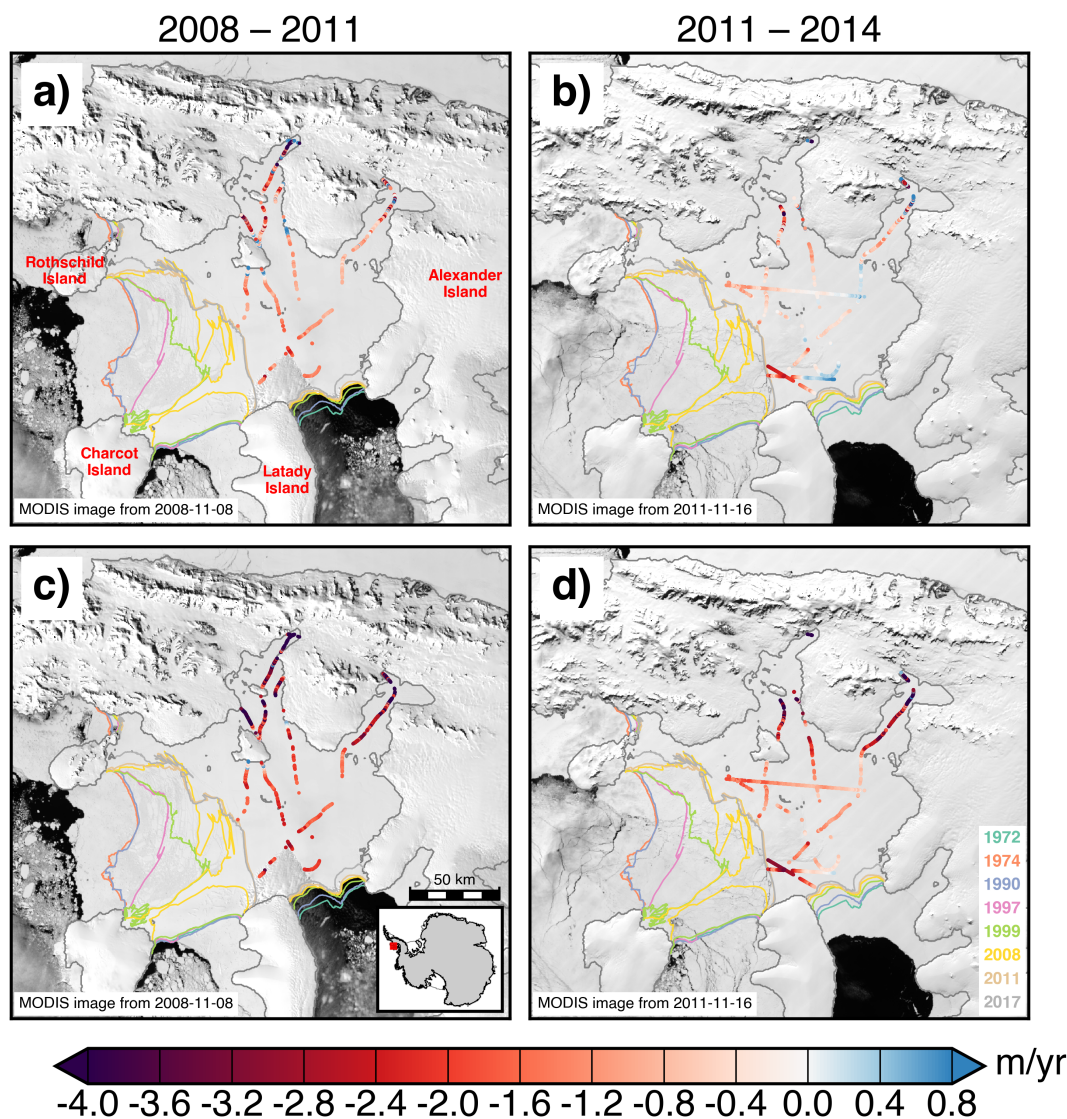
Figure 7. Ice thickness change (a-b) and estimated basal thickness change rates (c-d) of the Wilkins ice shelf for two periods, 2008–2011 and 2011–2014. MEaSUREs InSAR-derived Antarctic grounded ice boundaries are denoted in gray (Mouginot et al., 2017b). Historical ice shelf extents delineated from Landsat and MODIS imagery are denoted with colored lines (LPDAAC; Scambos et al., 2001). Plots are overlaid on MODIS images of Antarctic ice shelves provided by NSIDC (Scambos et al., 2001). Inset map denotes the location of the maps.
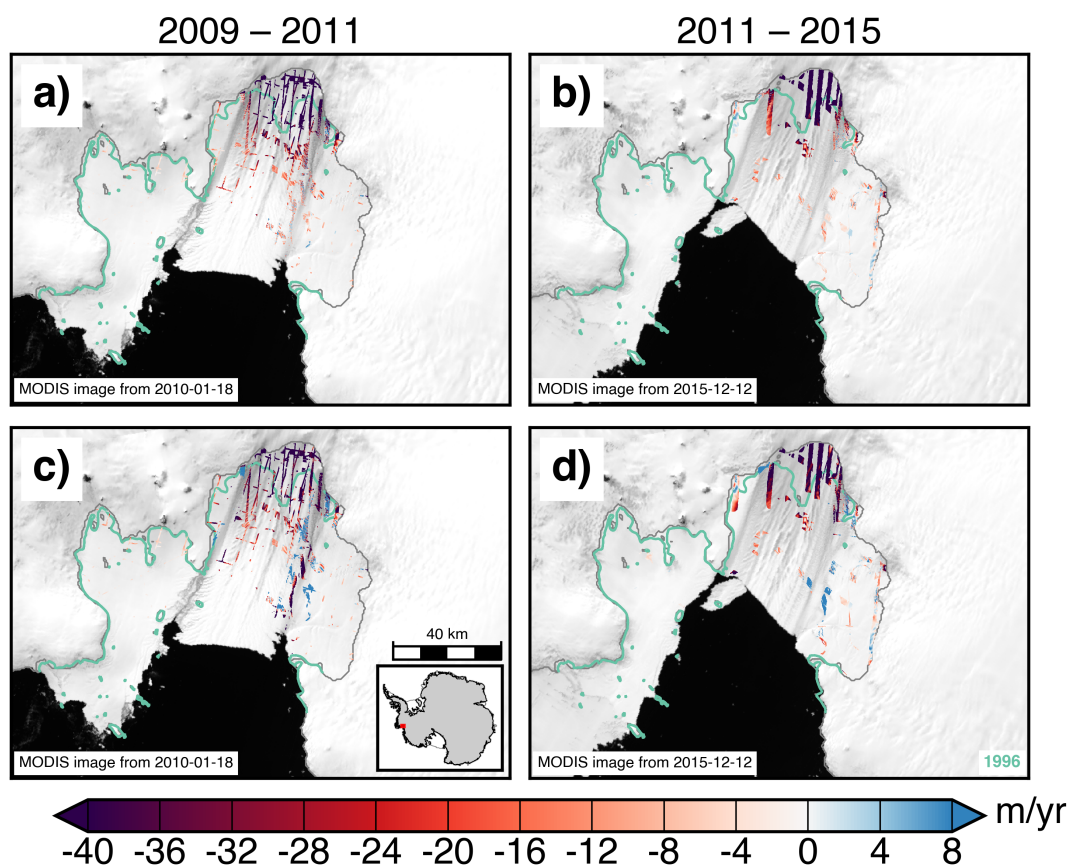
Figure 8. Ice thickness change (a-b) and estimated basal thickness change rates (c-d) of the Pine Island ice shelf for two periods, 2009–2011 and 2011–2015. MEaSUREs InSAR-derived Antarctic grounded ice boundaries are denoted in gray (Mouginot et al., 2017b). 1996 InSAR-derived grounding line locations from Rignot et al. (2016) are delineated in green. Plots are overlaid on MODIS images of Antarctic ice shelves provided by NSIDC (Scambos et al., 2001). Inset map denotes the location of the maps.
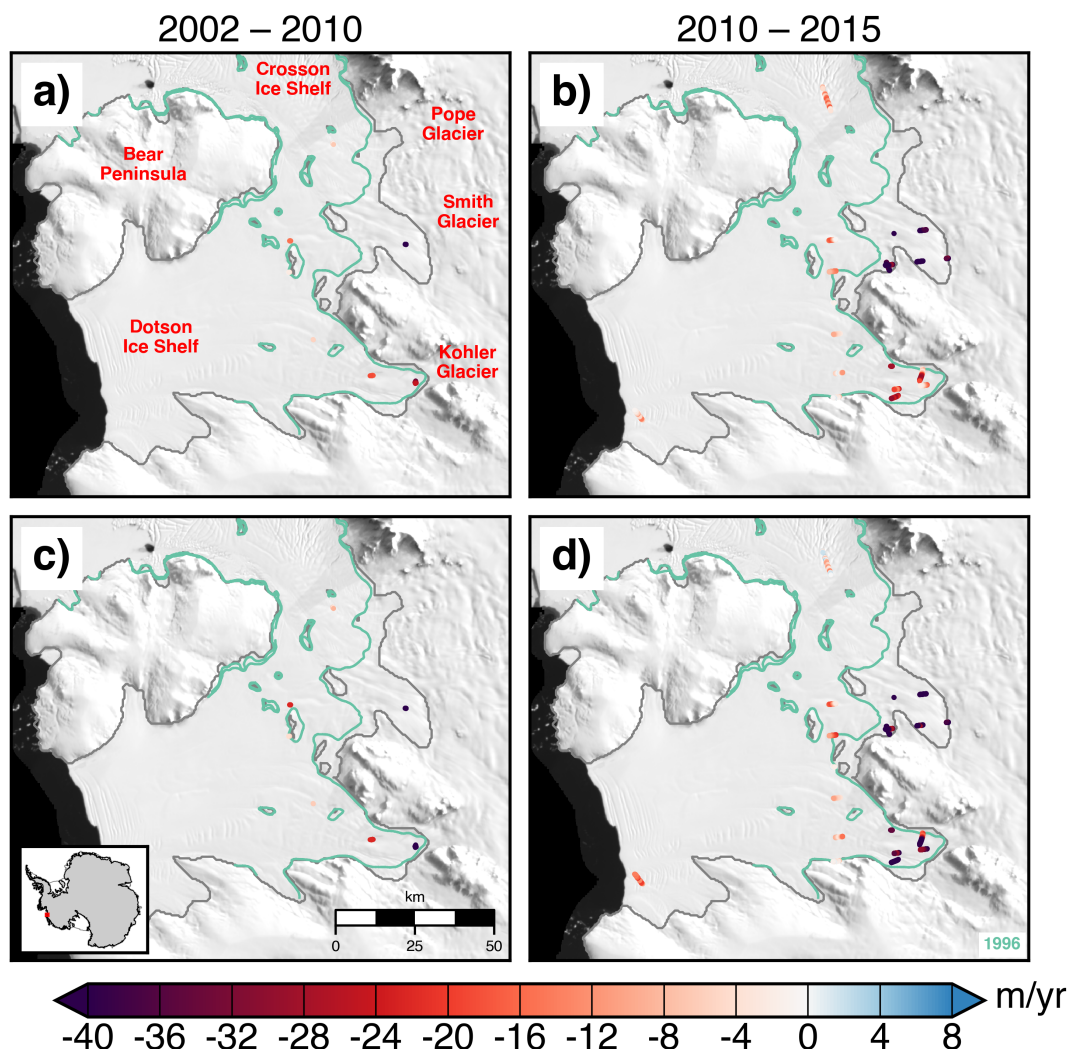
Figure 9. Ice thickness change (a-b) and estimated basal thickness change rates (c-d) of the Dotson and Crosson ice shelves for two periods, 2002–2010 and 2010–2015. MEaSUREs InSAR-derived Antarctic grounded ice boundaries are denoted in gray (Mouginot et al., 2017b). 1996 InSAR-derived grounding line locations from Rignot et al. (2016) are delineated in green. Plots are overlaid on a 2008–2009 MODIS mosaic of Antarctica (Haran et al., 2014). Inset map denotes the location of the maps.
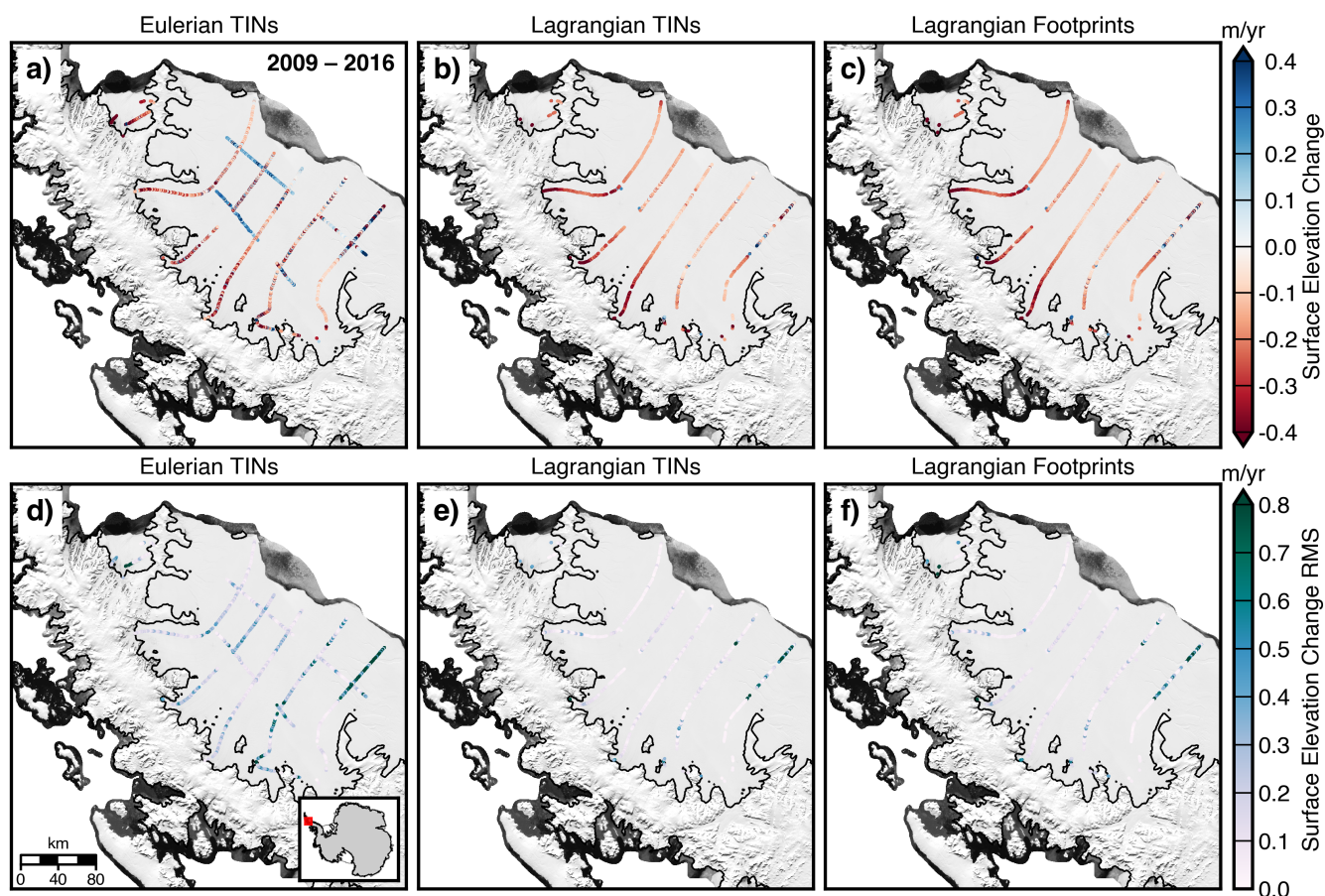
Figure 10. Surface elevation change of the Larsen-B remnant and Larsen-C ice shelf derived using a) Eulerian TINs, b) Lagrangian TINs and c) Lagrangian overlapping footprint schemes for the period 2009–2016. RMS differences in elevation change from a measurement point for all points within 1 km for the d) Eulerian TINs, e) Lagrangian TINs and f) Lagrangian overlapping footprint methods. The elevation change rates shown here are not corrected for oceanic or surface processes and are not RDE filtered (Smith et al., 2017). Antarctic grounded ice boundaries are provided by Mouginot et al. (2017b). Plots are overlaid on a 2008–2009 MODIS mosaic of Antarctica (Haran et al., 2014). Inset map denotes the location of the maps.